Interferences induced by spatially nonhomogeneous fields in high-harmonic generation

H. Ebadi

Max Planck Institute for Biophysical Chemistry, Am Fassberg 11, 37077 Göttingen, Germany

(Received 6 February 2014; revised manuscript received 14 April 2014; published 14 May 2014)

The high-harmonic spectrum simulated in a few-cycle laser pulse with spatially nonhomogeneous field presents two types of interferences, which characterize different plateaus in the spectrum. One of these plateaus is discernible with the nonequidistant peaks due to the interference of short and long trajectories, while another one is distinguished by a periodicity much larger than the laser frequency arising from trajectories modified by the nonhomogeneous field. Beside, the continuum-continuum harmonic generation appears in the spectrogram in the tunneling regime of the laser parameters. These features bear the tracking of classical trajectories and the complete characterization of emission spectrum, when using nanostructures in attoscience.

DOI: 10.1103/PhysRevA.89.053413 PACS number(s): 32.80.Wr, 33.20.Xx

I. INTRODUCTION

Since the invention of high-harmonic generation (HHG) using intense lasers, its generation and application have continuously been studied in attoscience [1]. Approaching the tunneling and barrier suppression ionization (BSI) regimes, this process is driven by classical trajectories (quantum orbits) [2–5]. The semiclassical formalism [6] explains HHG through these trajectories. In a linearly polarized intense laser with period T and periodic electric field $E(t)$, an electron when ionized at time t_i may return to the target potential at first return time $t_r^{i1} > t_i$ due to the change in the sign of the laser electric field. Then it may release its kinetic energy K^{i1} as HHG at first-order return, where the corresponding trajectories are called short and long trajectories. Moreover, some of these trajectories pass the target potential but they may return to it in another half cycle at the second return time $t_r^{i2} > t_r^{i1}$ and may release their kinetic energy K^{i2}. These trajectories are called second-order return trajectories. This scenario can be continued until the end of the laser pulse for each ionization moment. On the other hand, these released kinetic energies, known as bound-continuum (BC) harmonics, are generated via interference of the wave packet (WP) associated to these trajectories and the bound WP. In a long laser pulse, therefore, high-harmonics Ω should appear at odd multiples of laser frequency $\omega = 2\pi/T$ [7,8] up to $3.2U_p$, where $U_p = E_0/4\omega^2$ is the ponderomotive potential with $E_0 = \max(|E(t)|)$ (atomic units are used throughout unless otherwise stated). Furthermore, in HHG and also in the above-threshold ionization as its conjugate process of one-particle [9–17] and correlated few-particle dynamics [18], interference is one of the most important phenomena for analyzing observables. Now, in the few-cycle laser pulses as the key tool in attoscience, it is appropriate to interpret the structure of HHG spectra in terms of interferences by harmonic emission in the individual half cycles [5,9,13]. This approach describes the position of peaks, which may deviate from the odd harmonics. For instance, considering only first-order return trajectories with black dots in Fig. 1(a), the interference of harmonics in two consecutive half cycles with $t_r^{i1} - t_r^{j1} = \tau_2$ leads to a periodicity of $(2n+1)\omega$, whereas between two half cycles alternately with $t_r^{i1} - t_r^{j1} = \tau_1$ it induces periodicity of $n\omega$ with $n \in [0,1,2,\dots]$ in the spectrum. The signatures of these interferences have been observed from the attosecond pulse trains [11,12]. In addition, the interference of harmonics via short and long trajectories in the same half cycle with $t_r^{i1} - t_r^{j1} = \tau_3(\Omega)$ is another source for the deviation of peak positions from odd harmonics. This can be deduced from the cutoff region with nonequidistant peaks depending on the carrier envelope phase of the laser pulse [5,9,13] with the experimental evidence in Ref. [19]. Now taking into account HHG via second-order return trajectories [blue (gray) dots in Fig. 1(a)], whose contribution is usually negligible in the tunneling regime, two more characteristic energies should exist in the spectrum. The short or long trajectories in first return with those in the second return induce two-way interferences through either different or the same emission moments. The former induces a periodicity much larger than the laser frequency according to the smaller time distance between their return time ($t_r^{i1} - t_r^{j2} = \tau_4(\Omega) \simeq \tau_4$), while the latter result in the continuum-continuum (CC) HHG (vertical short-dashed light-blue [gray] arrows). These two features, however, are not usually discernible in a sinusoidal laser pulse due to the small probability and spreading of WP associated to the second- or higher-order return trajectories. Although few-cycle laser pulses are essential for controlling the electron dynamics [20], additional modification of the trajectories is required to observe these characteristic energies in HHG. This can be achieved with a spatially nonhomogeneous field synthesized from the sinusoidal laser pulse, which a lot of theoretical studies on HHG have recently been reported [21–26] following the experimental investigations [27–30]. In fact, these plasmonic fields, generated by using appropriate nanostructures, are suitable for the manipulation of light-matter interaction in advanced spectroscopy [31–33], generation of extreme-ultraviolet light [34,35], and HHG [27–30]. However, due to the overlap with emission from the excited atoms and related ionic species, the efficiency of HHG from a reduced sample volume is still not established [36–38] in this method. Using mid-infrared lasers, as reported recently [39–41], promises to increase the cutoff energy in HHG to distinguish the fluorescence emission of the excited atoms which occur below threshold. Moreover, these lasers allow one to use lower intensities, which may reduce thermal damage of the nanostructure and excitation of the ionic species and the related incoherent emission. On the other hand, since the theoretical simulation of HHG by nonhomogeneous fields is characterized by modified trajectories, also the analysis

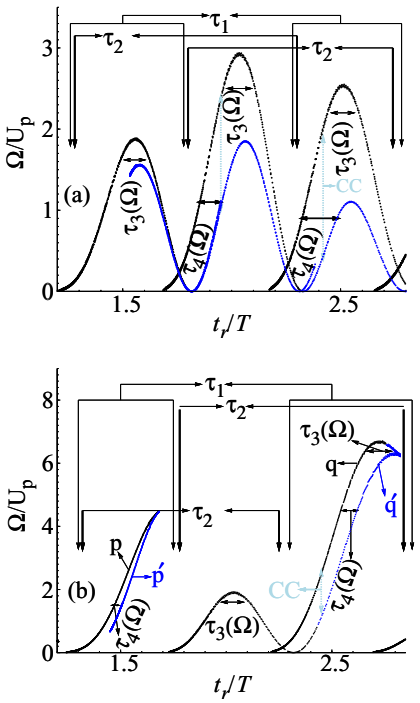

FIG. 1. (Color online) The classical prediction of return energies in HHG of an atom driven by a 4-cycle laser pulse for (a) homogeneous and (b) nonhomogeneous fields. τ_i with $i \in \{1,2,3,4\}$ indicates characteristic time distances corresponding to a certain periodicity in the spectrum as discussed in the text. For the convenience, the emission time is set $(T,3T)$. In panel (a), the emission by the first- and second-order return trajectories are shown with black and blue (gray) dots respectively. These symbols are employed for closed trajectories with earlier and later return times, respectively, modified by a spatially nonhomogeneous field, also marked with the same characters with and without prime (b). The vertical short-dashed light-blue (gray) arrows indicate CC transition.

of HHG in energy [10,29,30] and time [5,39] domains can prove and clarify the efficiency of the process. In this respect, there are reasonable suggestions for the experimental spectrum [30].

This work aims to study how interference fringes including even harmonics will appear in HHG spectra when modifying the classical trajectories by a spatially nonhomogeneous sinusoidal field. These fields induce close trajectories, marked with the same symbol but with and without prime in Fig. 1(b) $(q,q'$ and $p,p')$. The distance between their emission times is of the same order as the shortest distances between the emission times for the different return order trajectories in a sinusoidal pulse τ_4. Because of the probability of their WPs, it will be shown that a regular periodicity, which is larger than double the laser frequency, should appear in the corresponding HHG spectrum. For the same reason, the intensity of CC HHG [5,42] via these trajectories is discernible even in the tunneling regime of the laser field.

The theory and methods are presented in the next section. In Sec. III, the results are discussed and finally conclusions are give in Sec. IV.

II. THEORY AND METHODS

The theoretical investigation of high-harmonic generation and ionization in short laser pulses requires an appropriate form of the laser field to fulfill the fundamentals in the equation of motions. For the homogeneous case, the vector potential $\mathbf{A}(t)$ of a N-cycle laser pulse must obey $\mathbf{A}(t_d) - \mathbf{A}(0) = 0$, implying the zero dc component at the end of the laser pulse with a duration $t_d = NT$. In this work, an appropriate form of $\mathbf{A}(t)$ for a linearly polarized laser pulse is given by

$$\mathbf{A}(t) = \hat{e}_z A_0 f(t)\sin(\omega t + \phi), \tag{1}$$

where $\hat{e}_z$ indicates the polarization direction, A_0 is the vector potential peak, $f(t) = \sin^2(\pi t/t_d)$ is the envelope, ϕ is the carrier envelope phase, and N is the number of optical cycles of the laser pulse. Then, the corresponding electric field $\mathbf{E}(t)$ is obtained by $-\partial_t \mathbf{A}(t)/c$. Further, after combining a linearly polarized laser pulse with a simple linear function of coordinate $h(z) = \eta z$, which has been used in earlier studies [21–26], the spatially nonhomogeneous sinusoidal field reads

$$\mathbf{E}(z,t) = (1 + \eta z)\mathbf{E}(t). \tag{2}$$

Although there is no well-defined vector potential for $\mathbf{E}(z,t)$, one can present its impact when comparing the results obtained with a homogeneous one. As a target, the helium atom in the single active electron approximation has been chosen, for which the total Hamiltonian reads

$$\hat{H}(\mathbf{r},t) = \hat{H}_0(\mathbf{r}) + \mathbf{r}\cdot\mathbf{E}(z,t), \tag{3}$$

where

$$\hat{H}_0(\mathbf{r}) = -\tfrac{1}{2}\nabla^2 + V(\mathbf{r}) \tag{4}$$

is the field-free Hamiltonian containing the Laplacian operator and the screened electron-nuclear interaction $V(\mathbf{r})$. The model potential reported in Ref. [43] is employed, but the results do not depend on the other potentials [23,44]. With this Hamiltonian, the time-dependent Schrödinger equation $i\partial_t|\psi(\mathbf{r},t)\rangle = \hat{H}(\mathbf{r},t)|\psi(\mathbf{r},t)\rangle$ in the length gauge describes the quantum mechanical equation of motion. Having the ground state of $\hat{H}_0(\mathbf{r})$ from the standard techniques [45], the time-dependent wave function $|\psi(\mathbf{r},t)\rangle$ within the pulse length has been obtained by split-operator combined with Fourier spectral and Crank-Nicolson methods in the cylindrical coordinate system [5]. For the simulation of emission spectrum, either the dipole moment $\mathbf{d}(t) = \langle\psi(\mathbf{r},t)|\mathbf{r}|\psi(\mathbf{r},t)\rangle$ or preferentially the dipole acceleration $\ddot{\mathbf{d}}(t) = -\langle\psi(\mathbf{r},t)|\hat{\ddot{\mathbf{d}}}(\mathbf{r},t)|\psi(\mathbf{r},t)\rangle$ can be used with

$$\hat{\ddot{\mathbf{d}}}(\mathbf{r},t) = [\hat{H}(\mathbf{r},t),[\hat{H}(\mathbf{r},t),\mathbf{r}]]. \tag{5}$$

Then, their corresponding Fourier transforms $\tilde{\mathbf{d}}(\Omega) = FT[\mathbf{d}(t)]$ and $\tilde{\ddot{\mathbf{d}}}(\Omega) = FT[\ddot{\mathbf{d}}(t)]$ represent the power spectrum of HHG by $|S(\Omega)|^2$, where $S(\Omega)$ stands for $\tilde{\mathbf{d}}(\Omega)$ and $\tilde{\ddot{\mathbf{d}}}(\Omega)$. Further, the time-frequency analysis, given by

$$a_\sigma(\Omega_c,t) = \int S(\Omega)e^{-2\ln(2)\sigma^2(\Omega-\Omega_c)^2/2}e^{i\Omega t}d\Omega \tag{6}$$

at certain σ, expresses the role of quantum orbits in HHG.

Beside, modification of simple man's model [46] to the case of $\eta \neq 0$ provides the classical prediction of return energies, which examine the quantum results. Therefore, for a set of discrete ionization times t_i along a linearly polarized laser pulse, the one-dimensional classical equation of motion

$$\ddot{z(t)} = -\partial_z \mathbf{r} \cdot \mathbf{E}(z,t) \tag{7}$$

with $z(t_i) = 0$ and $\dot{z}(t_i) = 0$ as the initial conditions has numerically been solved to obtain the velocity $\dot{z}(t)$ and position $z(t)$ in $t > t_i$. The classical prediction of return energy for those trajectories, which return to the core, is given by their kinetic energy $\dot{z}(t_r)^2/2$ at their return time t_r.

III. RESULTS AND DISCUSSIONS

As discussed in Sec. I, when HHG beyond the multiphoton regime is driven by the classical trajectories, the spectrum structure is also characterized by these trajectories. Depending on the laser parameters, the structure of spectrum contains different fringes, which result from the interferences of BC HHG by these trajectories. However, there is no evidence of CC HHG by the classical trajectories in the spectrum structure but the time-frequency analysis allows one to observe these harmonics in the spectrogram. According to the importance of processes in an actual experimental measurement, this section begins with the analysis of the spectrum structure occurring via BC HHG and closes with the discussion on CC HHG. The simulations in this study have been done below the BSI regime with the similar parameters of Ref. [23] in a 4-cycle laser pulse with $\omega = 0.056$ and $E_0 = 0.19$. In fact, the general structure and the interpretation of the spectrum are independent of the laser frequency and intensity which were used in the earlier studies [39–41].

A. Interferences by modified trajectories

The earlier theoretical studies of HHG in a spatially nonhomogeneous field consider mainly the increasing cutoff energy and the multiplateau structure of the spectrum [21–23], but this investigation focuses on the analysis of the spectrum structure for which there is an experimental measurement for the case of a homogeneous field [19]. To this end a typical HHG spectrum is presented in Fig. 2, for which the same parameters were used as for Fig. 1(b), i.e., $\phi = \pi/4$, $\eta = 0.0029$, and $E_0 = 0.19$. This figure shows the multiplateaus and the increasing of the HHG cutoff compared to the case of sinusoidal homogeneous field, which have previously been reported in Refs. [21–23]. The former, however, can be divided to (0,2.7), (2.7,6.4), and (6.4,7.3) energy intervals in the unit of U_p. Surprisingly, the second and third plateaus above $2.7U_p$ can be clearly characterized by different interference fringes as shown by the linear scale in the inset. The second plateau shows a clear and almost constant periodicity ($\varpi \gg \omega$). This modulation should belong to the interference of HHG via close trajectories modified by a nonhomogeneous field. Moreover, in this plateau the spectrum contains a fine structure below $5U_p$, which is discussed subsequently. Although the relation between the cutoffs of each plateau and the harmonic emission from quantum orbits in the individual half cycles can be deduced from the classical predictions, this cannot easily be

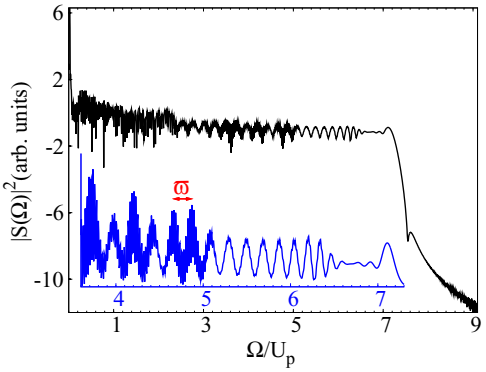

FIG. 2. (Color online) The log-scale HHG spectrum $|\tilde{\tilde{\mathbf{d}}}(\Omega)|^2$ (black line) simulated from the dipole acceleration in a 4-cycle laser pulse described through Eqs. (1) and (2) with $\eta = 0.0029$ and $\phi = \pi/4$. In the inset, the linear scale spectrum (blue [gray] line) from $2.5U_p$ to $7.5U_p$ shows two classes of interference fringes with high frequencies (below and above $6.4U_p$).

done for the interferences, because the probability of WP for the different trajectories, which cannot be obtained from the classical model, defines the interference structure of the spectrum. Thus, a time-frequency analysis of the spectrum is very useful, as shown in Fig. 3. One can see that the cutoff of the first plateau is identified by the harmonic emission at $2T$. The spectrum in this plateau has no structure due to HHG by several trajectories within the pulse length. But, according to the probability of harmonic emission, the second and third plateaus are characterized mainly by close trajectories whose emission time is in $(2.4T, 2.9T)$. The interference of harmonics by these trajectories, which induces a periodicity of ϖ in the spectrum, might be better understood via the superposition principle. To this end, the electric field of the emitted harmonics is represented by plane waves polarized in the z direction and propagated in the x direction:

$$\mathbf{E}_m(t) = \hat{e}_z A_m e^{i[kx+\Omega(t-t_r^m)]} \text{ in } t > t_r^m, \tag{8}$$

with $m \in \{q, q'\}$ ignoring the return orders. Here, the fields are assumed to be homogeneous, k is the wave number, and A_m is the amplitude of the emitted harmonic via trajectories. By

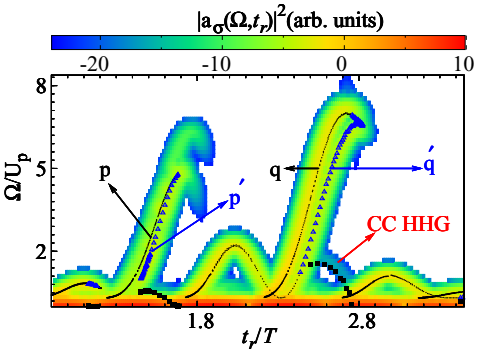

FIG. 3. (Color online) The spectrogram of the spectrum in Fig. 2 is superimposed with the classical predictions of return energies: black dots and blue (gray) triangles for BC HHG of trajectories with earlier and later return times, respectively, and black-filled squares for the corresponding CC HHG.

assuming real values for the amplitudes, the intensity of the emitted field attains the form

$$I(\Omega,t) \equiv |S(\Omega,t)|^2 = |A_q|^2 + |A_{q'}|^2 + 2A_q A_{q'}\cos(kx + \Omega\tau) \quad (9)$$

with $\tau = t_r^q - t_r^{q'} \equiv \tau_4$. Considering an interference term at $x = 0$, the maxima and minima of intensity in the energy domain appear at $2n\pi/\tau$ and $(2n+1)\pi/\tau$, respectively. Therefore, a periodicity of two times the difference of the closest maximum and minimum, i.e., $\varpi = 2\pi/\tau$, should appear in the spectrum. With $\varpi \approx 0.6 \gg \omega$ at around $3U_p$ one obtains $\tau \sim 10.4 \ll T = 112$, which is in good agreement with the classical counterpart $\tau_{\text{classic}} \approx 9.9$ a.u. (τ_4 in Fig. 1). As shown in Fig. 3, the harmonic emission by one of the two trajectories with later return time (q') ends up at around $6U_p$. Then, the sinusoidal-like curvature close to $6U_p$ smoothly increases the time distance between the emission moments of the two trajectories. This induces a smooth enhancement in the periodicity around this energy at the end of the second plateau in Fig. 2. Considering the time profile of attosecond pulses by using an appropriate filter [5] can be an alternative way for the actual measurement of this type of interference and modulation. The selection of trajectories and the time window can further be controlled by polarization gating approach [40].

In the third plateau above $6.4U_p$, the peak periodicity decreases with increasing harmonic energy. This is due to the interference of harmonics via short- and long-type trajectories in a half cycle analogous to those in the case of $\eta = 0$ [5,9,13]. As can be seen from classical predictions in Fig. 3, this plateau starts when HHG occurs via only one of these trajectories (q). Then, a small part of HHG via long trajectory around the cutoff induces nonequidistant peaks due to the interference with harmonics from short trajectories. Notably the distance between the emission times of short and long trajectories needs not necessarily be the same as that in the spatially homogeneous sinusoidal pulse. In this simulation, the energy range of this plateau is very small, but it varies when changing the laser parameters.

Looking at the spectrogram, there are other trajectories which emit harmonics above $2.7U_p$ at around $1.5T$ (p,p'). Hence, other fringes with characteristic energy close to ω are expected in the spectrum according to Eq. (6) with $\tau \sim t_r^q - t_r^{p'} \simeq 0.9T$ ignoring the return orders. This feature, which was related to τ_1 in Fig. 1(b), is clearly seen in Fig. 4, when enlarging the HHG spectra of Fig. 2 above $2.5U_P$. The peaks are approximately separated by $2\pi/0.9T = 0.062$ close to the driving laser frequency. Indeed, this equidistant periodicity, which also explains how the even harmonics in the spectrum appear [25,29,30], is very regular. Because only two short-type trajectories (e.g., p' and q) contribute in HHG, where their harmonic emission proceeds approximately parallel as a function of their return time. This regular structure is analog to the case when short and long trajectories are selected in an experiment to produce structured spectra in a spatially homogeneous laser pulse [10]. It is worth noting that the analog breaking of the Hamiltonian symmetry occurs on the two-color high-harmonic generation approach [47,48] for the spectral and temporal control of the attsoecond pulse trains. Therefore, the same applications in strong field

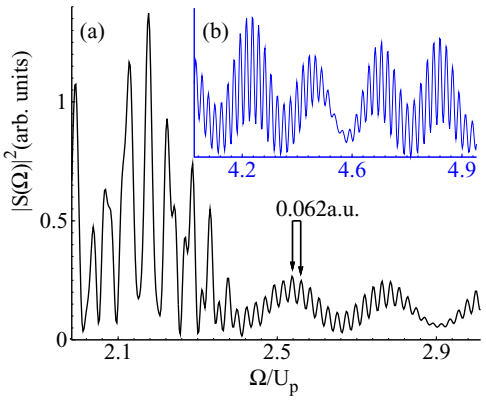

FIG. 4. (Color online) The enlargement of the spectrum in Fig. 2: (a) from 2 to 3 with black line and (b) from 4 to 5 with blue (gray) line in units of U_p.

ionization, which proposed for that scheme [49,50], can also be considered for the plasmonic field HHG. To close this subsection, the emitted spectrum has been compared with that obtained with homogeneous ($\eta = 0$) field in Fig. 5. For the homogeneous field, the cutoff energy again agrees with the classical prediction given in Fig. 1(a), when taking into account the ionization potential of the helium atom $I_P \simeq 0.9$. Regarding the spectrum structure, a few peaks above $3U_p$ arise via interference of harmonic emission from short and long trajectories in the middle of the pulse. An almost regular periodicity of 2ω in $(2.5U_p, 3.0U_p)$ is due to the interference of harmonic emission in the middle of the pulse and the next half cycle. But at lower energies, the spectrum becomes less structured, where it presents the interference of harmonic emission in several half cycles. The above discussions, in good agreement with the classical model, were based on the dipole acceleration. Because of the background, it has been verified that this form is more appropriate for the simulation and interpretation of the emitted spectrum [51,52]. In order to

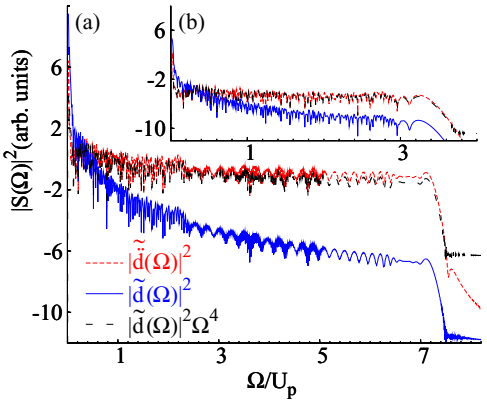

FIG. 5. (Color online) The log-scale HHG spectrum $|\tilde{\mathbf{d}}(\Omega)|^2$ simulated from the dipole moment (blue [gray], solid line) is superimposed with $|\tilde{\tilde{\mathbf{d}}}(\Omega)|^2$ (red [gray], short-dashed line) in a 4-cycle laser pulse described through Eqs. (1) and (2) with $\phi = \pi/4$; $\eta = 0.0029$ and $\eta = 0.0$ for panels (a) and (b), respectively. For the sake of clarity $|\tilde{\mathbf{d}}(\Omega)|^2$ has been scaled by a factor of Ω^4 with black long-dashed line.

consider this issue in the present work, the spectrum obtained from the induced dipole moment $|\tilde{\mathbf{d}}(\Omega)|^2$ is superimposed with $|\ddot{\tilde{\mathbf{d}}}(\Omega)|^2$ in this figure. Compared to the intensity in the plateau and cutoff region, the numerical background is several orders of magnitude lower for the case of dipole acceleration than for the case of dipole moment. There is also a discrepancy between them, when comparing $|\tilde{\mathbf{d}}(\Omega)|^2\Omega^4$ with $|\ddot{\tilde{\mathbf{d}}}(\Omega)|^2$. This discrepancy, which is more visible in the low-energy part for the case of homogeneous field, has been attributed to the influence of $\mathbf{d}(NT)$, $\dot{\mathbf{d}}(NT)$ [52], the CC and Raman-type transitions [51] in addition to the numerical background and reflection from the boundaries in the length form of the induced dipole moment. However, the spectra obtained with these two forms are still in excellent agreement, which indicates the efficient convergence of the quantum results.

B. CC HHG by modified trajectories

To accomplish the analysis of the emission processes, the discussion proceeds with the impact of a nonhomogeneous field on CC HHG, on which there are still no experimental reports. Considering two WPs with energies centered on E and E', the matrix element of $\hat{\mathbf{d}}(\mathbf{r},t)$ between these WPs reads

$$\langle\psi_E(\mathbf{r},t)|\hat{\mathbf{d}}(\mathbf{r},t)|\psi'_E(\mathbf{r},t)\rangle \approx \int_{E-\Delta E}^{E+\Delta E}\int_{E'-\Delta E}^{E'+\Delta E}\mathcal{F}(\epsilon,E)\mathcal{F}(\epsilon',E')c_\epsilon(t)c_{\epsilon'}(t)d_{\epsilon\epsilon'}(t)d\epsilon d\epsilon', \tag{10}$$

where $d_{\epsilon\epsilon'}(t)=\langle\nu_\epsilon(\mathbf{r})|\hat{\mathbf{d}}(\mathbf{r},t)|\nu_{\epsilon'}(\mathbf{r})\rangle e^{-i(\epsilon-\epsilon')t}$, $\nu_\epsilon(\mathbf{r})$ is virtual (atom-field) state with energy ϵ, and $\mathcal{F}(\epsilon,E)$ is a shape function presenting the distribution of virtual states around the central energy E. For the consistency, a small finite width $2\Delta E$ is assumed for the energy E. Now, if the WPs are considered to be the continuum as well as in the strong-field approximation [53], the resulting transition is called CC HHG [5,42]. For simplicity, with $\mathcal{F}(\epsilon,E)\approx\delta(\epsilon-E)$, the so-called Dirac δ function, this integral is reduced to

$$\langle\psi_E(\mathbf{r},t)|\hat{\mathbf{d}}(\mathbf{r},t)|\psi'_E(\mathbf{r},t)\rangle \approx \mathcal{W}(t)e^{-i(E-E')t}, \tag{11}$$

where $\mathcal{W}(t)=c_E(t)c_{E'}(t)d_{EE'}(t)$. The probability of WPs $c_E(t)$ has shown to be the most important factor in this expression, which induces a beat frequency $E-E'$ in the dipole acceleration. As CC HHG in the present laser parameters is also driven by quantum orbits, its highest intensity occurs when different quantum orbits with different energies return simultaneously to the target potential. Therefore, again one can calculate the classical prediction of CC HHG by $|K^q-K^{q'}|$ omitting the return order, although the transition is a pure quantum result. However, because of the lower intensity of CC HHG compared to BC, the time-frequency analysis is required to observe these harmonics. Looking at Fig. 3, one can see a clear signal for CC HHG with the classical counterpart, although the intensity of the laser pulse is in the tunneling regime. This is in contrast to the case of spatially homogeneous pulses, where an intensity in the BSI regime is required [5,42]. Here the excursion and thus the WP spreading of the trajectories together with cutoff energy are also modified by a nonhomogeneous field (e.g., for q and q') to observe a clear CC HHG. Hence, increasing the CC HHG by manipulating classical trajectories can be considered to be one of the important applications of the nonhomogeneous fields in the experimental investigations. While the CC HHG is hidden in the spectrum, in the presence of a phase matching, considering the resulting attosecond pulses should be the most appropriate way for an actual measurement and experimental investigation of these harmonics [5].

IV. CONCLUSIONS

In summary, the spatially nonhomogeneous field applied in the few-cycle laser pulse induces additional periodicities in the HHG spectrum. These periodicities, explaining the origin of even harmonics, have arisen from interference of harmonics via classical trajectories. Thus the structure of spectrum can be used for tracking these trajectories, when they will be modified using nanostructures. In addition, the intensity of CC transition is enhanced in the tunneling regime of the laser intensity, which is appropriate for experimental investigation of these harmonics in attoscience. This work presents a step toward the full characterization of the plasmonic-field-driven high-harmonic generation.

ACKNOWLEDGMENT

Useful comments and discussions with E. Lötstedt and support by MPI-BPC are gratefully acknowledged.

[1] F. Krausz and M. Ivanov, Rev. Mod. Phys. **81**, 163 (2009).
[2] D. B. Milošević, G. G. Paulus, and W. Becker, Phys. Rev. A **71**, 061404(R) (2005).
[3] L. Brugnera, D. J. Hoffmann, T. Siegel, F. Frank, A. Zair, J. W. G. Tisch, and J. P. Marangos, Phys. Rev. Lett. **107**, 153902 (2011).
[4] L. E. Chipperfield, P. L. Knight, J. W. G. Tisch, and J. P. Marangos, Opt. Commun. **264**, 494 (2006).
[5] H. Ebadi, Opt. Commun. **315**, 226 (2014).
[6] M. Lewenstein, Ph. Balcou, M. Yu. Ivanov, A. L'Huillier, and P. B. Corkum, Phys. Rev. A **49**, 2117 (1994).
[7] F. Ceccherini and D. Bauer, Phys. Rev. A **64**, 033423 (2001).
[8] O. E. Alon, V. Averbukh, and N. Moiseyev, Phys. Rev. Lett. **80**, 3743 (1998).
[9] A. deBohan, P. Antoine, D. B. Milošević, and B. Piraux, Phys. Rev. Lett. **81**, 1837 (1998).
[10] G. Sansone, E. Benedetti, J.-P. Caumes, S. Stagira, C. Vozzi, M. Pascolini, L. Poletto, P. Villoresi, S. De Silvestri, and M. Nisoli, Phys. Rev. Lett. **94**, 193903 (2005).
[11] E. Mansten, J. M. Dahlström, J. Mauritsson, T. Ruchon, A. L'Huillier, J. Tate, M. B. Gaarde, P. Eckle, A. Guandalini, M. Holler, F. Schapper, L. Gallmann, and U. Keller, Phys. Rev. Lett. **102**, 083002 (2009).
[12] X. He, J. M. Dahlström, R. Rakowski, C. M. Heyl, A. Persson, J. Mauritsson, and A. L'Huillier, Phys. Rev. A **82**, 033410 (2010).

[13] M. V. Frolov, N. L. Manakov, A. A. Silaev, N. V. Vvedenskii, and A. F. Starace, Phys. Rev. A **83**, 021405(R) (2011).
[14] P. Johnsson, J. Mauritsson, T. Remetter, A. L'Huillier, and K. J. Schafer, Phys. Rev. Lett. **99**, 233001 (2007).
[15] O. I. Tolstikhin, Phys. Rev. A **77**, 032712 (2008).
[16] H. Ebadi, C. H. Keitel, and K. Z. Hatsagortsyan, Phys. Rev. A **83**, 063418 (2011).
[17] H. Ebadi, J. Opt. Soc. Am. B **29**, 2503 (2012).
[18] L. Argenti and E. Lindroth, Phys. Rev. Lett. **105**, 053002 (2010).
[19] T. Auguste, P. Salières, A. S. Wyatt, A. Monmayrant, I. A. Walmsley, E. Cormier, A. Zaïr, M. Holler, A. Guandalini, F. Schapper, J. Biegert, L. Gallmann, and U. Keller, Phys. Rev. A **80**, 033817 (2009).
[20] E. Lötstedt and K. Midorikawa, Phys. Rev. A **88**, 041402 (2013).
[21] B. Fetić, K. Kalajdžić, and D. B. Milošević, Ann. Phys. **525**, 107 (2013).
[22] M. F. Ciappina, J. Biegert, R. Quidant, and M. Lewenstein, Phys. Rev. A **85**, 033828 (2012).
[23] J. A. Pérez-Hernández, M. F. Ciappina, M. Lewenstein, L. Roso, and A. Zaïr, Phys. Rev. Lett. **110**, 053001 (2013).
[24] M. F. Ciappina, S. S. Acimovic, T. Shaaran, J. Biegert, R. Quidant, and M. Lewenstein, Opt. Exp. **20**, 26261 (2012).
[25] M. F. Ciappina, T. Shaaran, and M. Lewenstein, Ann. Phys. **525**, 97 (2013).
[26] T. Shaaran, M. F. Ciappina, R. Guichard, J. A. Pérez-Hernández, L. Roso, M. Arnold, T. Siegel, A. Zaïr, and M. Lewenstein, Phys. Rev. A **87**, 041402(R) (2013).
[27] S. Kim, J. Jin, Y.-J. Kim, I.-Y. Park, Y. Kim, and S.-W. Kim, Nature (London) **453**, 757 (2008).
[28] N. Pfullmann, C. Waltermann, M. Noack, S. Rausch, T. Nagy, C. Reinhardt, M. Kovaev, V. Knittel, R. Bratschitsch, D. Akemeier, A. Hütten, A. Leitenstorfer, and U. Morgner, New J. Phys. **15**, 093027 (2013).
[29] I.-Y. Park, S. Kim, J. Choi, D.-H. Lee, Y.-J. Kim, M. F. Kling, M. I. Stockman, and S.-W. Kim, Nat. Photon. **5**, 677 (2011).
[30] I.-Y. Park, J. Choi, D.-H. Lee, S. Han, S. Kim, and S.-W. Kim, Ann. Phys. **525**, 87 (2013).
[31] D. A. Genov, A. K. Sarychev, V. M. Shalaev, and A. Wei, Nano Lett. **4**, 153 (2004).
[32] P. J. Schuck, D. P. Fromm, A. Sundaramurthy, G. S. Kino, and W. E. Moerner, Phys. Rev. Lett. **94**, 017402 (2005).
[33] P. Mühlschlegel, H.-J. Eisler, O. J. F. Martin, B. Hecht, and D. W. Pohl, Science **308**, 1607 (2005).
[34] M. Sivis and C. Ropers, Phys. Rev. Lett. **111**, 085001 (2013).
[35] M. Sivis, M. Duwe, B. Abel, and C. Ropers, Nat. Phys. **9**, 304 (2013).
[36] M. Sivis, M. Duwe, B. Abel, and C. Ropers, Nature (London) **485**, E1 (2012).
[37] S. Kim, J. Jin, Y.-J. Kim, I.-Y. Park, Y. Kim, and S.-W. Kim, Nature (London) **485**, E2 (2012).
[38] I. Yavuz, Phys. Rev. A **87**, 053815 (2013).
[39] J. Luo, Y. Li, Z. Wang, L. He, Q. Zhang, P. Lan, and P. Lu, Phys. Rev. A **89**, 023405 (2014).
[40] L. Feng, M. Yuan, and T. Chu, Phys. Plasmas. **20**, 122307 (2013).
[41] J. Luo, Y. Li, Z. Wang, Q. Zhang, and P. Lu, J. Phys. B: At. Mol. Opt. Phys. **46**, 145602 (2013).
[42] M. C. Kohler, C. Ott, P. Raith, R. Heck, I. Schlegel, C. H. Keitel, and T. Pfeifer, Phys. Rev. Lett. **105**, 203902 (2010).
[43] H. G. Muller, Phys. Rev. Lett. **83**, 3158 (1999).
[44] X. M. Tong and C. D. Lin, J. Phys. B **38**, 2593 (2005).
[45] H. Ebadi, Comput. Phys. Commun. **184**, 550 (2013).
[46] H. B. van Linden van den Heuvell and H. G. Muller, in *Multiphoton Processes*, edited by S. J. Smith and P. L. Knight (Cambridge University Press, Cambridge, England, 1988).
[47] E. Mansten, J. M. Dahlström, P. Johnsson, M. Swoboda, A. L'Huillier, and J. Mauritsson, New J. Phys. **10**, 083041 (2008).
[48] J. M. Dahlström, A. L'Huillier, and J. Mauritsson, J. Phys. B: At. Mol. Opt. Phys. **44**, 095602 (2011).
[49] J. Mauritsson, P. Johnsson, E. Gustafsson, A. L'Huillier, K. J. Schafer, and M. B. Gaarde, Phys. Rev. Lett. **97**, 013001 (2006).
[50] J. Mauritsson, P. Johnsson, E. Mansten, M. Swoboda, T. Ruchon, A. L'Huillier, and K. J. Schafer, Phys. Rev. Lett. **100**, 073003 (2008).
[51] J. L. Krause, K. J. Schafer, and K. C. Kulander, Phys. Rev. A **45**, 4998 (1992).
[52] K. Burnett, V. C. Reed, J. Cooper, and P. L. Knight, Phys. Rev. A **45**, 3347 (1992).
[53] L. V. Keldysh, JETP **47**, 1945 (1964) [Sov. Phys. JETP **20**, 1307 (1965)].